Available online at www.sciencedirect.com
ScienceDirect
Journal of Power Sources 167 (2007) 529–535
JOURNAL OF POWER SOURCES
www.elsevier.com/locate/jpowsour

Short communication

Novel SnS_2-nanosheet anodes for lithium-ion batteries

Tae-Joon Kim, Chunjoong Kim, Dongyeon Son, Myungsuk Choi, Byungwoo Park *

Department of Materials Science and Engineering, Research Center for Energy Conversion and Storage, Seoul National University, Seoul, Republic of Korea

Received 28 November 2006; accepted 10 February 2007
Available online 27 February 2007

Abstract

Crystalline tin-sulfide nanosheets are synthesized through a one-step solvothermal process and incorporated in the negative electrode material for lithium-ion batteries. SnS_2 compounds synthesized in ethylene glycol have an approximately 2 nm-thick nanosheet morphology and exhibit an excellent charge-capacity retention of ~95% after 50 cycles between 1.15 and 0 V at 0.5 C (=323 mA g^{-1}). The thickness of the nanosheets is varied up to ~26 nm by adjusting the precursors, solvents and source concentrations. The nanostructural effects are investigated in terms of electrochemical and rate-capability properties.

Keywords: SnS_2 anode; Nanosheet; Solvothermal process; Lithium-ion battery; Capacity retention; Nanostructural effects

1. Introduction

Further improvement of the specific energy of lithium-ion batteries is required for the next generation of electronic devices. The carbon negative electrode (anode) that is presently used in commercial batteries (with a theoretical capacity of 372 mAh g^{-1}) is insufficient to meet the future needs of high capacity. Recently, various metal composites, metal oxides and metal sulfides – based on their transformation to lithium-metal alloys – have been studied extensively as possible alternatives to carbonaceous anode materials because of their higher capacities [1–5].

The SnS_2 compound has a layered hexagonal CdI_2-type crystal structure ($a = 0.3648$ nm, $c = 0.5899$ nm, space group $P\bar{3}m1$) that consists of two layers of close-packed sulfur anions with tin cations sandwiched between them in an octahedral coordination. The adjacent sulfur layers are bound by weak van der Waals interactions [6]. The electrochemical reaction mechanisms of SnS_2 with lithium have been proposed to be [2]:

$$SnS_2 + 4Li^+ + 4e^- \rightarrow Sn + 2Li_2S \quad (1)$$

$$Sn + xLi^+ + xe^- \leftrightarrow Li_xSn\ (0 \le x \le 4.4). \quad (2)$$

On the first discharge, lithiation leads to the decomposition of SnS_2 into metallic tin and Li_2S. During substantial charge and discharge, tin alloys/dealloys up to the theoretical limit of $Li_{4.4}Sn$ (i.e., a capacity of 645 mAh g^{-1}), and Li_2S acts as an inert matrix that surrounds the active Sn grains [2].

Unfortunately, the capacity fading of Sn-based electrode materials is severe due to large volume changes (over 300%) during cycling [7,8]. An effective way to improve the cycling stability of Sn-based materials is to reduce their particle size to the nanometer range [9,10]. Various methods have been developed for the synthesis of SnS_2 nanostructures with different sizes (from ~10 to ~100 nm) and morphologies such as nanoparticles, nanorods, nanobelts, nanotubes, and nanosheets [11–17].

Effects of tin-sulfide anodes with a nanostructure size of the order of just a few nm have not been reported due to the limits of nanostructural control, and their electrochemical properties have not been satisfactory [2,3,18–20]. In this study, ultra-thin SnS_2 nanosheets (with a thickness down to 2 nm) are synthesized via a simple catalyst-free solvothermal route. The nanosheets are successfully applied to electrochemical reactions, with good electronic connectivity (compared with nanoparticles) and fast reaction kinetics.

* Corresponding author. Tel.: +82 2 880 8319; fax: +82 2 885 9671.
E-mail address: byungwoo@snu.ac.kr (B. Park).

0378-7753/$ – see front matter © 2007 Elsevier B.V. All rights reserved.
doi:10.1016/j.jpowsour.2007.02.040

2. Experimental

2.1. Synthesis 1

Stannic chloride ($SnCl_4$, 0.15 ml) and solid sulfur (S, 0.2 g) were added to ethylene glycol ($C_2H_6O_2$, 100 ml) in a Teflon-lined, stainless-steel autoclave and stirred for 10 min. The mixture was maintained in an oven at 160–200 °C for 24 h. After cooling to room temperature, SnS_2-nanosheet precipitates were obtained from the solution through centrifugal filtration. The precipitates were washed with ethanol and distilled water several times to remove the organic residues, and then dried for 10 h at 60 °C.

2.2. Synthesis 2

To obtain SnS_2 nanosheets with a wider variation of thickness, various source concentrations of stannous chloride dihydrate ($SnCl_2{\cdot}2H_2O$) and thiourea ($(NH_2)_2CS$) in benzene (50 ml) were used, such as 25, 50, 125 and 250 mM. The mixture was placed in an autoclave that was maintained in an oven at 185 °C for 20 h. After cooling, the centrifugal filtration, washing and drying processes were performed as described above.

3. Characterization and electrochemical properties

X-ray diffraction (XRD) with Cu $K\alpha$ radiation (M18XHF-SRA, MAC Science) was used to determine the phase composition and the crystallinity. The sizes and morphologies of the nanosheets were observed by transmission electron microscopy (TEM: JEM-3000F, JEOL), by dispersion in ethanol.

Electrochemical cycling tests were performed with coin-type half-cells (2016 size). The working electrode was made from the SnS_2-nanosheet active material, super P carbon black, and a polyvinylidene fluoride (PVdF) binder in a weight ratio of 60:20:20 on a copper foil. The electrolyte was 1 M $LiPF_6$ with 1:1 ethylene carbonate:diethylene carbonate (EC:DEC), and the counter and reference electrodes were made from lithium foil. The cycle-life of the cells was tested at a rate of 0.5 C (=323 mA g^{-1}, 1 C = 645 mA g^{-1}) within a fixed voltage window of 1.15–0 V. The rate capability was evaluated by varying the discharge rate from 0.2 to 5 C. Cyclic voltammetry was performed to examine the cathodic reaction (reduction) and the anodic reaction (oxidation) in the voltage range of 2.5–0 V (versus Li/Li^+), at a sweep rate of 0.05 mV s^{-1}.

4. Results and discussion

4.1. Synthesis of SnS_2 nanosheets (synthesis 1)

To minimize residuals and impurities, simple reactants were used in synthesis 1. As described above, the SnS_2 nanosheets were successfully synthesized by a one-step polyol method without using any other surfactant/functional groups [16,17]. Ethylene glycol acts as a reducing agent by capping the Sn ion sources, and leads to the formation of a polymeric network by preventing the aggregation of the nanosheets [21]. After hydrolysis and washing out of the ethylene glycol, SnS_2 nanostructures are obtained.

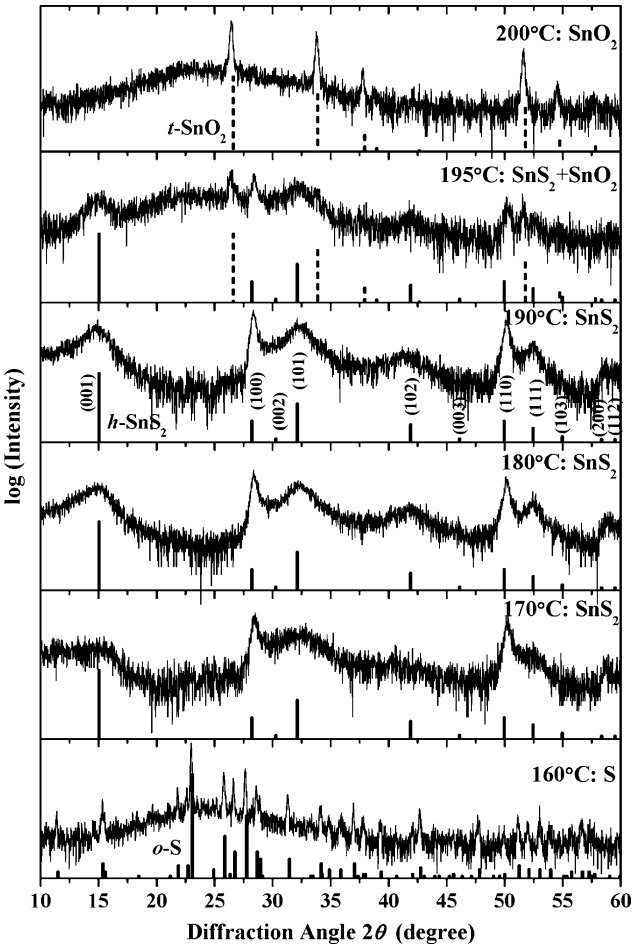

Fig. 1. X-ray diffraction patterns of SnS_2 nanostructures synthesized at various temperatures (from synthesis 1). Ideal peak positions and intensities for hexagonal SnS_2 (JCPDS #23-0677) tetragonal SnO_2 (JCPDS #41-1445), and orthorhombic S (JCPDS #08-0247) are marked.

The XRD patterns of the precipitates prepared at various temperatures are shown in Fig. 1; the broad peak at ~25° is associated with the glass holder. The diffractions of the products synthesized at 170, 180 and 190 °C clearly correspond to hexagonal β-SnS_2. The sample synthesized at 170 °C exhibits poor crystallinity and a more defective structure compared with those produced at 180 and 190 °C. The products synthesized at 195 °C contain a mixture of SnS_2 and tetragonal SnO_2 phases, and full oxidation to SnO_2 is observed at 200 °C, which may be due to the thermal decomposition of ethylene glycol (boiling point: 195–197 °C).

Clearly, the crystalline tin sulfides obtained at 170, 180 and 190 °C have an anisotropic nanosheet structure. The effective crystallite sizes were calculated by the Scherrer equation from the broadening of the (0 0 1) and (1 0 0) peaks in the XRD patterns (Table 1) [22–24]. The nanosheets synthesized at 180 and 190 °C are each estimated to have a thickness of 2.0 ± 0.1 nm in [0 0 1], while that synthesized at 170 °C has a thickness of 1.6 ± 0.1 nm. The TEM images (Fig. 2) of the as-prepared

Table 1
Effective crystallite sizes calculated by Scherrer equation from X-ray diffraction of synthesized SnS_2 nanosheets

	Synthesis condition	[0 0 1] Direction (nm)	[1 0 0] Direction (nm)
Synthesis 1 [$SnCl_4$ + S + ethylene glycol]	170 °C	1.6 ± 0.1	16.6 ± 1.0
	180 °C	2.0 ± 0.1	17.4 ± 0.6
	190 °C	2.0 ± 0.1	19.1 ± 0.6
Synthesis 2 [$SnCl_2{\cdot}2H_2O + (NH_2)_2CS$ + benzene]	25 mM	3.2 ± 0.5	41.3 ± 4.3
	50 mM	10.4 ± 0.2	42.5 ± 1.9
	125 mM	17.5 ± 0.3	48.9 ± 2.2
	250 mM	25.6 ± 0.2	70.4 ± 1.7

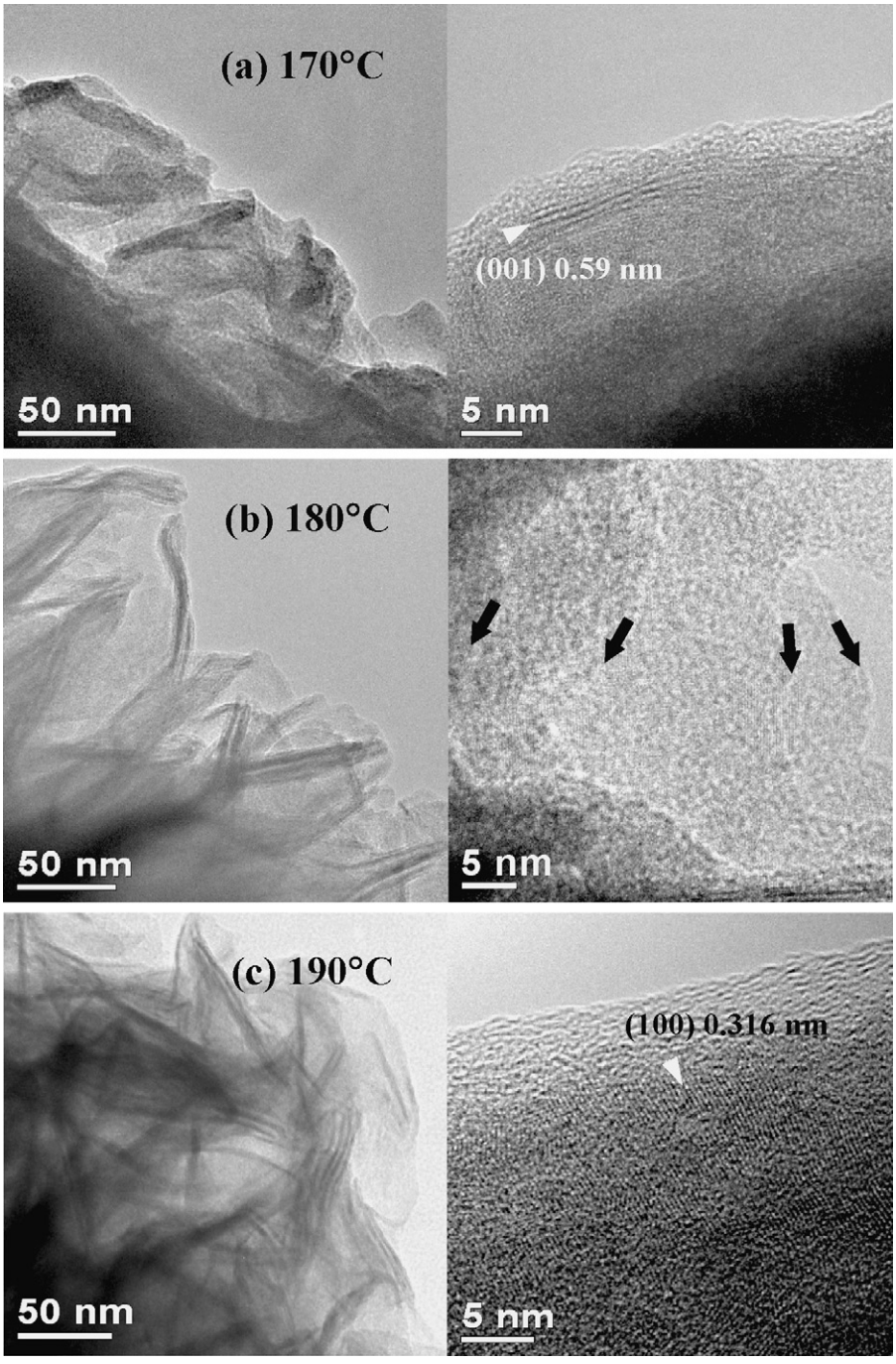

Fig. 2. Transmission electron micrographs of SnS_2 nanosheets synthesized at (a) 170 °C, (b) 180 °C and (c) 190 °C (from synthesis 1). Black arrows indicate edges of peeled nanosheets from overlapped multi-nanosheets.

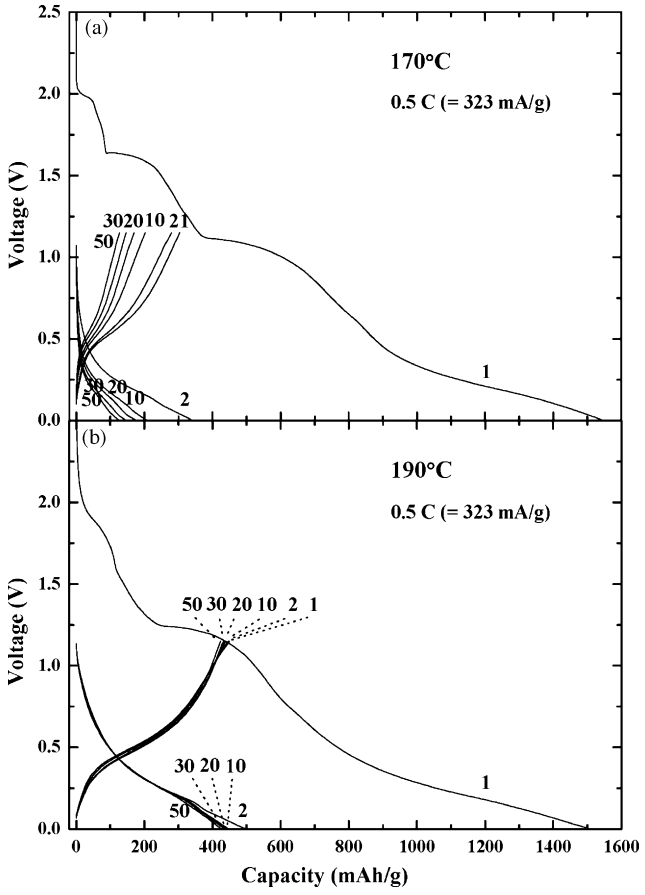

Fig. 3. Voltage profiles of SnS_2 nanosheets synthesized at (a) 170 °C and (b) 190 °C (from synthesis 1), between 1.15 and 0 V.

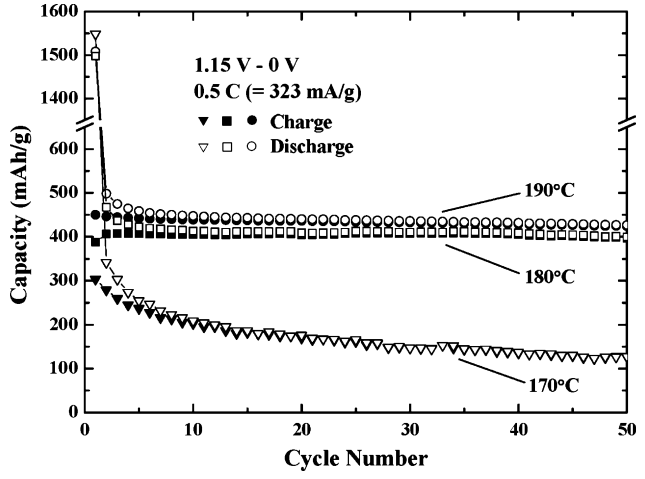

Fig. 4. Cycle-life performance of SnS_2-nanosheet anodes synthesized at 170, 180 and 190 °C (from synthesis 1).

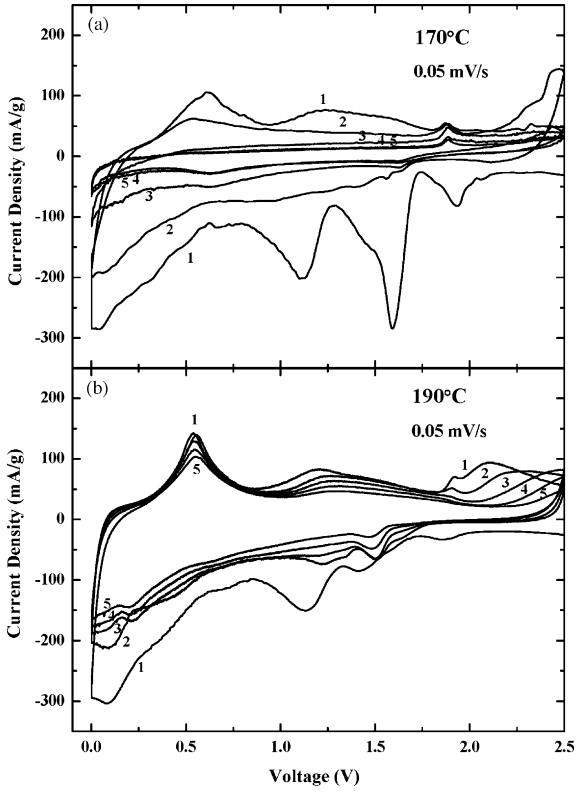

Fig. 5. Cyclic voltammograms of SnS_2-nanosheet anodes synthesized at (a) 170 °C and (b) 190 °C (from synthesis 1).

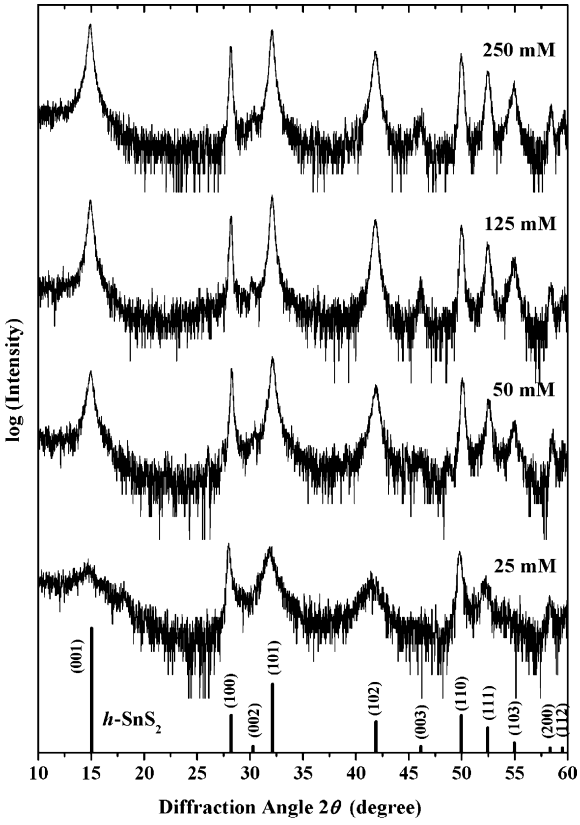

Fig. 6. X-ray diffraction patterns of synthesized SnS_2 nanosheets with various source concentrations (from synthesis 2). Ideal peak positions and intensities for hexagonal SnS_2 (JCPDS #23-0677) are marked.

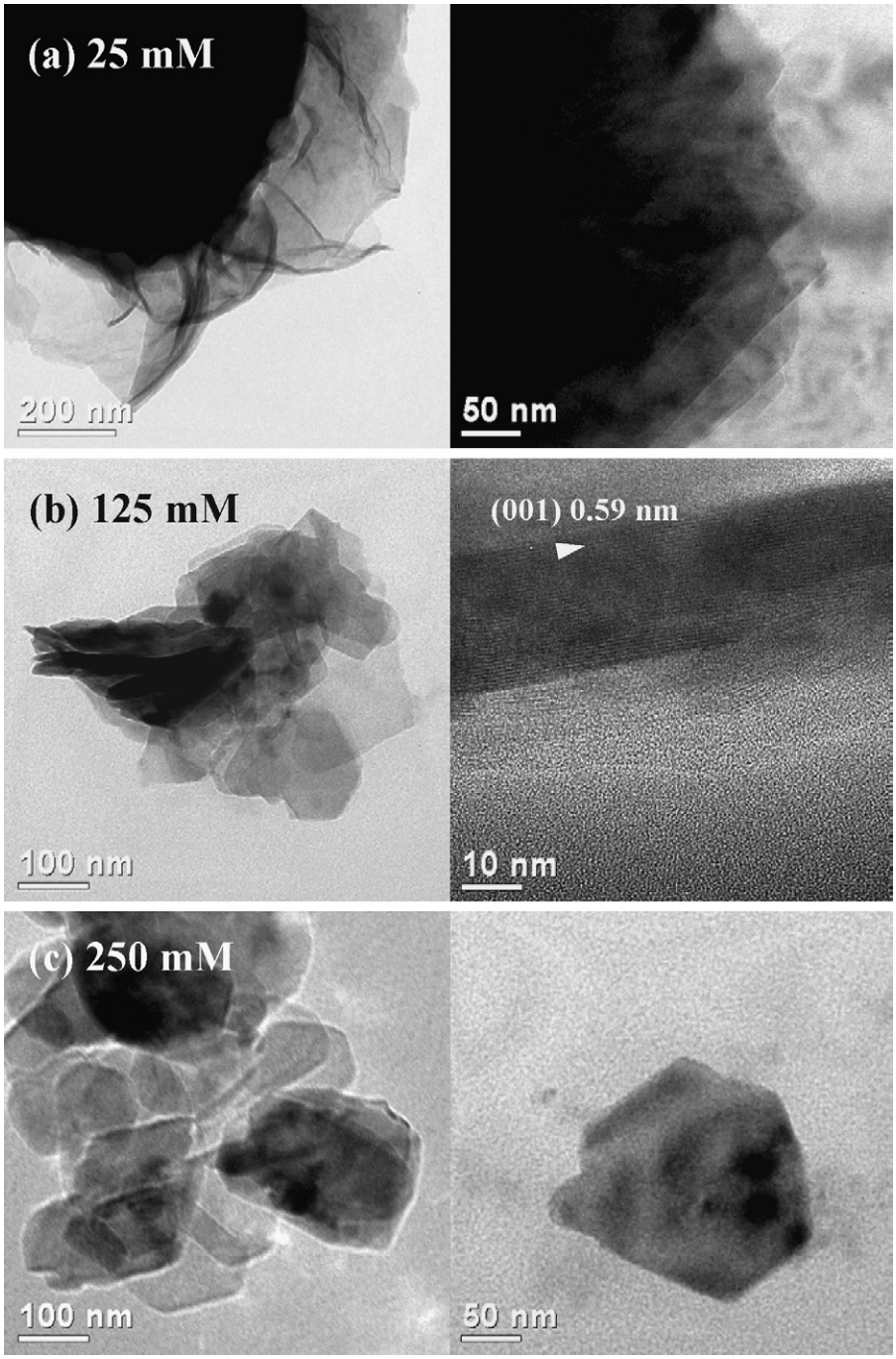

Fig. 7. Transmission electron micrographs of SnS_2 nanosheets synthesized at (a) 25 mM, (b) 125 mM and (c) 250 mM (from synthesis 2).

products exhibit overall thin nanosheet morphologies. The samples at 180 and 190 °C consist of long layer-rolled and undulating sheets, as compared with the sample at 170 °C which is made up of relatively short stumpy flakes. The (0 0 1) and (1 0 0) lattice planes are clearly seen, as well as the presence of overlapping multi-nanosheets that have the appearance of partly-peeled onion skins.

Electrochemical cycling tests of the nanosheet-SnS_2 electrodes were performed at 0.5 C between 1.15 and 0 V. The voltage profiles of the cells using the 170 and 190 °C samples for 50 cycles are presented in Fig. 3(a and b), respectively. (The voltage profiles of the 180 °C sample, which are not shown, are similar to those of the 190 °C sample.) The 170 °C sample (with the smallest thickness) exhibits three obvious plateau at ~1.95, ~1.65 and ~1.1 V on the first discharge, while the 190 °C sample has a more diffuse first-discharge profile [3]. According to reactions (1) and (2), the first-discharge capacity (i.e., the sum of the irreversible and reversible capacities) should be 1232 mAh g^{-1}. For both samples, however, the excessive first-discharge capacity is ~300 mAh g^{-1}. The high surface-to-volume ratio of the nanostructure and/or the abundance of surface defects may accelerate side-reactions with the electrolytes and cause some

irreversible trapping of lithium. As can be seen from cycle-life data (Fig. 4), the SnS_2-nanosheet anodes synthesized at 180 and 190 °C give excellent capacity retention (i.e., ~95% after 50 cycles). A deficient level of crystallinity may be the cause of the poor cyclability of the 170 °C sample.

Cyclic voltammograms of the SnS_2-nanosheet anodes synthesized at 170 and 190 °C for five cycles are presented in Fig. 5. The broad peak at ~1.1 V in the first cathodic sweep has been reported to correspond to the reaction (1), while those at ~0.1 V in the first cathodic scan and at ~0.6 V in the first anodic scan are known to represent the redox peak couple of reaction (2) [2,3,19]. In the case of nanosheets with an extremely small thickness (especially in the 170 °C sample), however, unreported additional peaks are observed at ~1.6 and ~1.9 V in the first cathodic scan, and are also partially reversible. According to previous reports [25–27], lithium can intercalate to some extent into the SnS_2 layers without causing phase decomposition and, consequently, reaction (1) may be subdivided into three steps as follows:

$$SnS_2 + xLi^+ + xe^- \rightarrow Li_xSnS_2 \quad (3)$$

$$Li_xSnS_2 + (y-x)Li^+ + (y-x)e^- \rightarrow Li_ySnS_2 \quad (4)$$

$$Li_ySnS_2 + (4-y)Li^+ + (4-y)e^- \rightarrow Sn + 2Li_2S\,(0 < x < y \leq 2). \quad (5)$$

The peaks at ~1.9, ~1.6 and ~1.1 V in the first cathodic scan of the 170 °C sample can be considered as the proposed reactions (3)–(5), respectively. Nevertheless, it is considered that the mechanisms of electrochemical lithium insertion into SnS_2 require further study.

4.2. Size variation of SnS_2 nanosheets (synthesis 2)

Non-polar benzene solvent is more suitable for obtaining nanosheets with a larger grain size, while the thiourea complex acts as a capping agent in the same way as that of ethylene glycol in synthesis 1. SnS_2 nanosheets with various thicknesses ranging from ~3 to ~26 nm were obtained by adjusting the source concentration (Fig. 6 and Table 1). As shown in the TEM images of Fig. 7, the thick nanosheets obtained at a higher source concentration have a decreased aspect ratio, while the nanosheets obtained at a lower source concentration are thin and wide. This means that a higher source concentration leads to more flocculation and the thin layers are stable without breakage of the wide connections in the solvent medium.

Results from electrochemical cycling of SnS_2 nanosheets with various thicknesses are presented in Fig. 8(a). The anode made with nanosheets having a thickness of ~10 nm (50 mM) retains about 93% of the charge capacity after 50 cycles. The corresponding value for nanosheets with thicknesses of ~18 nm (125 mM) and ~26 nm (250 mM) are ~83% and ~63%. In comparison with the nanosheets formed at 190 °C in synthesis 1 (approximately 2 nm thickness with ~95% capacity retention), the thickness of the nanosheets is correlated with the cycle-life performance.

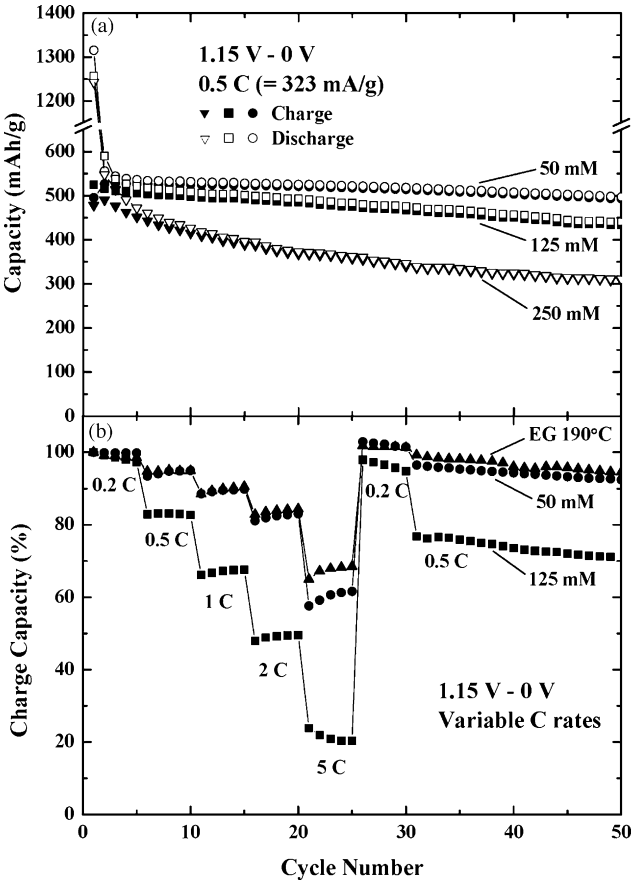

Fig. 8. (a) Cycle-life performance of SnS_2 nanosheets synthesized at 50, 125 and 250 mM (from synthesis 2). (b) Rate-capability test of SnS_2 nanosheets synthesized at 50 and 125 mM (from synthesis 2), and at 190 °C (from synthesis 1).

Data from rate-capability tests (from 0.2 to 5 C, between 1.15 and 0 V) of SnS_2 anodes with different nanosheet sizes are give in Fig. 8(b). The rate capability depends on the nanosheet thickness. At the 5 C rate, nanosheets prepared at 50 mM (~10 nm thickness) and 125 mM (~18 nm thickness) in synthesis 2 retain ~60% and ~20% of the initial 0.2 C capacity, respectively, while those formed at 190 °C (~2 nm thickness) in synthesis 1 retain ~70%. Thus, nanosheets with a small thickness are advantageous in terms of fast reaction kinetics.

5. Conclusions

Crystalline SnS_2 nanosheets with thicknesses that range from ~1.6 to ~26 nm have been successfully prepared via a one-step solvothermal process. Electrochemical cycling tests confirm that thinner nanosheets are more advantageous with respect to reaction kinetics, and that nanosheets with thicknesses from ~2 to ~10 nm exhibit an excellent capacity retention of over 90% after 50 cycles. Detailed mechanisms of the electrochemical insertion of lithium into SnS_2 require further elucidation.

Acknowledgements

The authors wish to thank Tae-Gon Kim and Joon-Gon Lee for their assistance with TEM and XRD measurements,

and Cheil Industries for the supply of electrolytes. The work was supported by the ERC program of MOST/KOSEF (R11-2002-102-00000-0), and by the Basic Research Program (R01-2004-000-10173-0) of KOSEF.

References

[1] H. Li, X. Huang, L. Chen, Solid State Ionics 123 (1999) 189–197.
[2] T. Brousse, S.M. Lee, L. Pasquereau, D. Defives, D.M. Schleich, Solid State Ionics 113–115 (1998) 51–56.
[3] T. Momma, N. Shiraishi, A. Yoshizawa, T. Osaka, A. Gedanken, J. Zhu, L. Sominski, J. Power Sources 97–98 (2001) 198–200.
[4] T.-J. Kim, D. Son, J. Cho, B. Park, H. Yang, Electrochim. Acta 49 (2004) 4405–4410.
[5] T. Moon, C. Kim, S.-T. Hwang, B. Park, Electrochem. Solid-State Lett. 9 (2006) A408–A411.
[6] F. Lévy, Crystallography and Crystal Chemistry of Materials with Layered Structures, Reidel, Dordrecht, 1976, pp. 2–3.
[7] I.A. Courtney, J.R. Dahn, J. Electrochem. Soc. 144 (1997) 2943–2948.
[8] S. Bourdeau, T. Brousse, D.M. Schleich, J. Power Sources 81–82 (1999) 233–236.
[9] N. Li, C.R. Martin, B. Scrosati, Electrochem. Solid-State Lett. 3 (2000) 316–318.
[10] C. Kim, M. Noh, M. Choi, J. Cho, B. Park, Chem. Mater. 17 (2005) 3297–3301.
[11] X.F. Qian, X.M. Zhang, C. Wang, W.Z. Wang, Y. Xie, Y.T. Qian, J. Phys. Chem. Solids 60 (1999) 415–417.
[12] H. Su, Y. Xie, Y. Xiong, P. Gao, Y. Qian, J. Solid State Chem. 161 (2001) 190–196.
[13] Y. Ji, H. Zhang, X. Ma, J. Xu, D. Yang, J. Phys.: Condens. Matter 15 (2003) L661–L665.
[14] D. Chen, G.-Z. Shen, K.-B. Tang, Y.-K. Liu, Y.-T. Qian, Appl. Phys. A 77 (2003) 747–749.
[15] Q. Li, Y. Ding, H. Wu, X. Liu, Y. Qian, Mater. Res. Bull. 37 (2002) 925–932.
[16] G. Shen, D. Chen, K. Tang, L. Huang, Y. Qian, G. Zhou, Inorg. Chem. Commun. 6 (2003) 178–180.
[17] D. Chen, G. Shen, K. Tang, S. Lei, H. Zheng, Y. Qian, J. Cryst. Growth 260 (2004) 469–474.
[18] H. Mukaibo, A. Yoshizawa, T. Momma, T. Osaka, J. Power Sources 119–121 (2003) 60–63.
[19] X.-L. Gou, J. Chen, P.-W. Shen, Mater. Chem. Phys. 93 (2005) 557–566.
[20] Y. Li, J.P. Tu, H.M. Wu, Y.F. Yuan, D.Q. Shi, Mater. Sci. Eng. B 128 (2006) 75–79.
[21] G. Zhang, M. Liu, J. Mater. Sci. 34 (1999) 3213–3219.
[22] B.E. Warren, X-Ray Diffraction, Addison-Wesley, Reading, 1969, pp. 257–258.
[23] P. Scherrer, Gottinger Nachrichten 2 (1918) 98–100.
[24] T. Kim, J. Oh, B. Park, K.S. Hong, Appl. Phys. Lett. 76 (2000) 3043–3045.
[25] J. Morales, C. Perez-Vicente, J.L. Tirado, Solid State Ionics 51 (1992) 133–138.
[26] C. Julien, C. Perez-Vicente, Solid State Ionics 89 (1996) 337–343.
[27] I. Lefebvre-Devos, J. Oliver-Fourcade, J.C. Jumas, P. Lavela, Phys. Rev. B 61 (2000) 3110–3116.